Terahertz semiconductor-heterostructure lasers

Rüdeger Köhler, Alessandro Tredicucci, Fabio Beltram
NEST-INFM & Scuola Normale Superiore, Piazza dei Cavalieri 7, 56126 Pisa, Italy

Harvey E. Beere, Edmund H. Linfield, A. Giles Davies, David A. Ritchie
Cavendish Laboratory, University of Cambridge, Madingley Road, Cambridge CB3 0HE, United Kingdom

Rita C. Iotti, Fausto Rossi
INFM & Dipartimento di Fisica, Politecnico di Torino, Corso Duca degli Abruzzi 24, 10129 Torino, Italy

Abstract: Injection lasers based on interminiband transitions in GaAs/AlGaAs heterostructures are operated in the THz range. Single-mode emission is achieved at 4.4THz, with output powers of 2.5mW and thresholds of few hundred A/cm^2 up to 50K.
©2002 Optical Society of America
OCIS Codes: (140.3070) Infrared and far-infrared lasers; (140.5960) Semiconductor lasers

1. Introduction

The terahertz region (1-10 THz) of the electromagnetic spectrum offers ample opportunities in spectroscopy, free space communications, remote sensing and medical imaging. Yet, the use of THz waves in all these fields has been limited by the lack of appropriate, convenient sources. Existing solid-state emitters, in fact, lack the general requisites of compactness, integrability and portability necessary for implementation in actual devices, and suffer from low output powers, limited tunability, and/or the necessity of liquid helium cryogenics.

Research on THz semiconductor lasers has received new life in the last few years thanks to the development of quantum cascade (QC) lasers of ever increasing wavelength [1,2]. However, fundamental problems related to the transition energy being below the optical phonon resonance and to confinement of the emitted radiation have seriously hampered the realization of THz QC devices.

With the help of detailed theoretical modeling and the adoption of a partially metallic waveguide, we have demonstrated a monolithic THz heterostructure laser based on interminiband transitions in the conduction band of a GaAs/AlGaAs QC heterostructure. Single mode emission is achieved at 4.4 THz ($\lambda \sim$ 67 μm) with high output powers of more than 2.5 mW. Although operation is presently limited to 50 K, the low threshold current density of less than 300 A/cm^2 underlines the great development potential of the present concept for continuous-wave and high-temperature operation, which should soon lead to implementation in real-world photonic systems.

2. Design and modeling

Electrons in a QC laser propagate through a potential staircase of coupled quantum wells, where the conduction band is split by quantum confinement into a number of distinct subbands. By choice of layer thickness and applied electric field, lifetimes and tunneling probabilities of each level are engineered in order to obtain population inversion between two such subbands in a series of identical repeat units, allowing in principle operation at arbitrarily small energies. Although THz electroluminescent devices have been reported by several groups [3,4], laser action was possible only at much shorter wavelengths, above the material *reststrahlenband.* Up until now, proposed THz QC designs have featured narrow injector minibands to suppress scattering of electrons from the upper laser state through LO-phonon emission. As a consequence, extraction of carriers from the lower laser level is very slow, which, compounded with the limited current densities supported, hinders the achievement of population inversion. Our design targets precisely these two issues, an objective best fulfilled by the adoption of chirped superlattice active regions [5]. One repeat unit in our structure comprises seven GaAs quantum wells separated by $Al_{0.15}Ga_{0.85}As$ barriers, with the active region consisting of three closely-coupled quantum wells. A self-consistent calculation of the wavefunctions and energies is shown in Fig. 1a, and details of the design are given in the caption. The optical transition takes place across the 18 meV wide minigap between the second and first miniband (states 2 and 1) and, being vertical in real space, presents a large dipole matrix element of 7.8 nm. The lower laser state 1 is strongly coupled to a wide injector miniband, comprising seven

subbands spanning an energy of 17 meV. This provides a large phase space where electrons scattered either from subband 2 or directly from the injector can spread, at the same time ensuring fast depletion of state 1. Moreover, the wide miniband allows efficient electrical transport and simultaneously suppresses thermal backfilling. The validity of this design is supported by theoretical modeling employing a Monte-Carlo scheme based on a coupled set of fully three-dimensional Boltzmann equations, including all relevant energy-relaxation mechanisms [6]. The results predict the build-up of a significant population inversion above an applied electric field of 2kV/cm, peaking at about 1.5 x 10^9 cm^{-2} just before the design field of 3.5 kV/cm. Large current densities of the order of 1 kA/cm^2 are also obtained before the onset of negative differential resistance that marks the end of resonant tunneling transport.

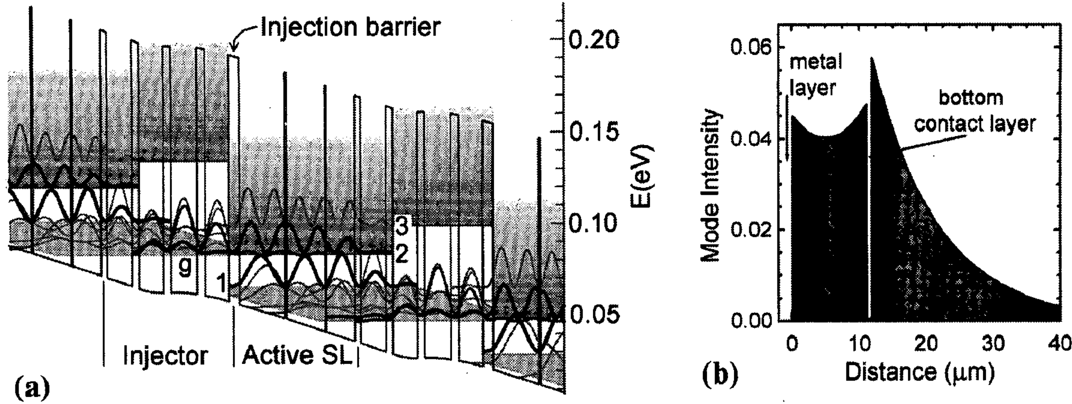

Fig. 1. (a) Self-consistent calculation of the conduction band structure of a portion of the layer stack in the waveguide core under a field of 3.5 kV/cm. The layer thickness, in nm, starting from the injection barrier are **4.3**/18.8/**0.8**/15.8/**0.6**/11.7/**2.5**/10.3/**2.9**/10.2/**3.0**/10.8/**3.3**/9.9, where $Al_{0.15}Ga_{0.85}As$ layers are in bold face and the 10.2 nm wide well is Si-doped at 4 × 10^{16} cm^{-3}. The moduli squared of the wavefunctions are shown, with miniband regions represented by shaded areas. (b) Calculated mode profile along the growth direction of the final device structure. The origin of the abscissa is at the top metal-semiconductor interface and the shaded area indicates the waveguide core of 104 repetitions of the injector-active SL unit shown in panel (a).

The waveguide is also a very important aspect of the present device. Traditionally long-wavelength QC lasers exploit the surface plasmon mode at the interface between two materials with dielectric constants of opposite sign (normally a metal and a semiconductor) to achieve a tight optical confinement with low absorption losses [2,7]. At THz frequencies, however, a simple surface-plasmon waveguide results in a small overlap of the optical mode with any active region of reasonable thickness. We have thus chosen to use a thin (800 nm) n^+ GaAs layer between 104 repeat periods of the above active superlattice on one side and an undoped GaAs substrate on the other in order to create a strongly confined low loss TM mode bound to that layer. This is a result of the n^+ layer dielectric constant (ε_A), which, by appropriately tuning the doping density, can be made negative, albeit comparable in modulus to the one (ε_B) of the surrounding semiconductor. The two surface plasmons existing at the two layer interfaces merge into a single mode and the penetration into the outside semiconductor is at the same time minimized. We chose a donor density $n = 2 \times 10^{18}$ cm^{-3}, which yields a good compromise between absorption losses and overlap with the active material. Additionally this makes it possible to use the n^+ layer for electrical contacting. The presence on top of the active regions of a 200 nm thick GaAs layer doped to $n = 5 \times 10^{18}$ cm^{-3} with its metallic contact leads to the final mode profile of the actual device shown in Fig. 1b. A confinement factor $\Gamma = 0.47$ for the active material and an attenuation coefficient $\alpha_W = 16$ cm^{-1} are computed, both extremely favorable values at these long wavelengths.

3. Experimental results

The sample was grown by molecular beam epitaxy and the wafer was processed into mesa-etched ridge stripes by optical lithography and wet chemical etching. Top and bottom Ge/Au ohmic contacts were provided by thermal evaporation, and a Fabry-Perot cavity was formed by cleaving the stripes into laser bars. The devices were finally soldered onto a copper block, wire-bonded, and mounted onto the cold finger of a liquid-He flow cryostat. Current macro-pulses were applied at a repetition rate of 333 Hz and matched the frequency response of the detector; each macro-pulse comprised 750 micro-pulses of width up to 250 ns

at intervals of 2 μs to avoid excess heating in the device. The emitted radiation was collected by an f/1 off-axis parabolic mirror, passed through a Fourier transform interferometer (FTIR), and focused again onto a liquid-He cooled Si bolometer. Laser spectra were collected with a DTGS (deuterated triglycine sulfate) detector.

Figure 2a shows the 8 K emission spectra of a 1.2 mm long, 180 μm wide laser for different drive currents. The characteristic narrowing of the emission line, and non-linear dependence of the intensity, are clearly observed up to a current of about 880 mA, where laser threshold is reached. Lasing takes place at ≈ 4.4 THz, on the high-energy side of the luminescence line, probably owing to the reduced waveguide losses at shorter wavelengths. Single-mode emission is obtained, most likely a consequence of the relatively narrow gain spectrum and the wide Fabry-Perot mode spacing. A high-resolution laser spectrum is shown in the inset of Fig. 2a; the measured linewidth is limited by the resolution of the spectrometer (3.75 GHz).

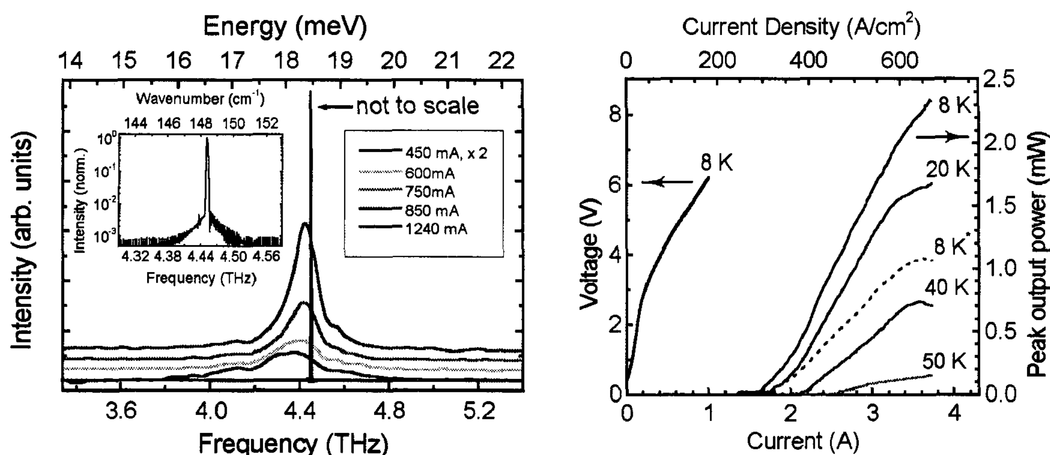

Fig. 2. (Left panel) Emission spectra from a 1.2 mm long laser device for different drive currents as recorded at 8 K. The lowest curve is multiplied by a factor of two for clarity. The 1240 mA laser spectrum was scaled down by several orders of magnitude. Inset: The laser line on a logarithmic scale. (Right panel) Light-current (L-I) characteristics of a 180 μm wide and 3.1 mm long laser ridge. Data was recorded applying 100 ns long pulses at a repetition rate of 333 Hz. Increasing the duty-cycle to 0.5 % the peak power reduces to 1 mW as is shown by the dashed curve labeled with an asterisk. The V-I curve at a temperature of 8 K is also displayed.

Fig. 2b shows the light-current (L-I) and voltage-current (V-I) characteristics of a 3 mm long device. At a heat-sink temperature of 8 K, the output peak power is estimated to be more than 2 mW, with a threshold current density of 290 A/cm^2. The latter is a very small value for QC lasers, and allows operation at high duty cycles (up to 10 %) even in this large-size device. We expect that narrower stripes and appropriate changes in sample processing will lead to continuous-wave operation. The threshold current increases with temperature up to the maximum operating temperature of 55 K. Current-voltage characteristics are similar to those observed in mid-infrared QC structures. From the theoretical values of population inversion and confinement factor, we compute a maximum modal gain of 23 cm^{-1}. This value compares well with the estimated cavity losses $\alpha_W + \alpha_M = (16 + 4)$ cm^{-1} = 20 cm^{-1}, α_M being the mirror out-coupling of the 3 mm long stripe.

4. References

[1] J. Faist *et al.*, "Quantum Cascade Laser", *Science* **264**, 553-556 (1994).
[2] R. Colombelli *et al.*, "Far-infrared surface-plasmon quantum-cascade lasers at 21.5 μm and 24 μm wavelengths", *Appl. Phys. Lett.* **78**, 2620-2622 (2001).
[3] M. Rochat, J. Faist, M. Beck, U. Oesterle, M. Ilegems, "Far-infrared (λ = 88 μm) electroluminescence in a quantum cascade structure", *Appl. Phys. Lett.* **73**, 3724-3726 (1998).
[4] J. Ulrich, R. Zobl, W. Schrenk, G. Strasser, K. Unterrainer, "Terahertz quantum cascade structures: intra- versus interwell transition", *Appl. Phys. Lett.* **76**, 1928-1930 (2000).
[5] A. Tredicucci *et al.*, "High performance interminiband quantum cascade lasers with graded superlattices", *Appl. Phys. Lett.* **73**, 2101-2103 (1998).
[6] R. Köhler, R. C. Iotti, A. Tredicucci, F. Rossi "Design and simulation of terahertz quantum cascade lasers", *Appl. Phys. Lett.* **79**, 3920-3922 (2001).
[7] C. Sirtori *et al.*, "Long-wavelength (λ ~ 8 - 11.5 μm) semiconductor lasers with waveguides based on surface plasmons", *Opt. Lett.* **23**, 1366-1368 (1998).